Cell Systems

Report

# Synthetically programmed antioxidant delivery by a domesticated skin commensal

## Graphical abstract

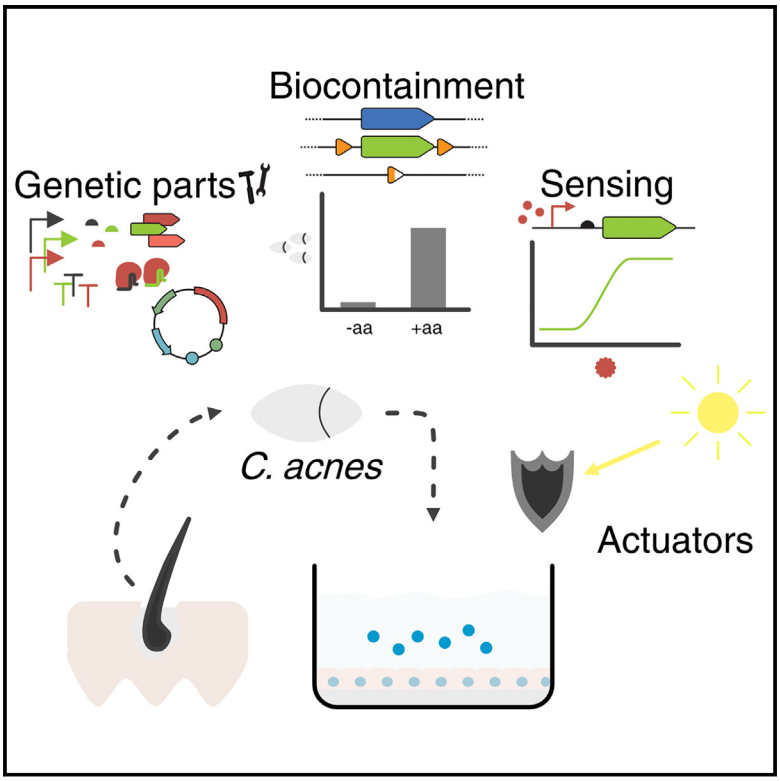


## Highlights

- *C. acnes* genetic toolkit for skin microbiome research and applications
- CRISPRi for fast prototyping of auxotrophies for biocontainment
- Adaptation and *de novo* discovery of regulators allows dynamic sensing in *C. acnes*
- Antioxidant-secreting *C. acnes* reduces oxidative stress in a UV stress model

## Authors

Guillermo Nevot,
Javier Santos-Moreno,
Nil Campamà-Sanz, ...,
Rodrigo Ledesma-Amaro,
Ellen H. van den Bogaard, Marc Güell

## Correspondence

javier.santos@upf.edu (J.S.-M.),
marc.guell@upf.edu (M.G.)

## In brief

Nevot, Santos-Moreno, et al. develop a synthetic biology toolbox for engineering *Cutibacterium acnes*, the dominant skin commensal, as a chassis for live biotherapeutics. Demonstrating auxotrophic biocontainment and environmental sensing, the engineered strains secrete antioxidants to mitigate UV-induced oxidative stress, paving the way for innovative microbiome-based skin therapies.

Nevot et al., 2025, Cell Systems *16*, 101169
February 19, 2025 
https://doi.org/10.1016/j.cels.2025.101169

CellPress

Cell Systems

CellPress
OPEN ACCESS

Report

# Synthetically programmed antioxidant delivery by a domesticated skin commensal

Guillermo Nevot,[1,6] Javier Santos-Moreno,[1,6,*] Nil Campamà-Sanz,[3] Lorena Toloza,[1] Cristóbal Parra-Cid,[1] Patrick A.M. Jansen,[4] Içvara Barbier,[5] Rodrigo Ledesma-Amaro,[5] Ellen H. van den Bogaard,[4] and Marc Güell[1,2,7,*]

[1]Department of Medicine and Life Sciences, Universitat Pompeu Fabra, 08003 Barcelona, Cataluña, Spain
[2]ICREA, Institució Catalana de Recerca i Estudis Avançats, 08003 Barcelona, Cataluña, Spain
[3]Department of Cell and Molecular Biology, Karolinska Institutet, Södermanland and Uppland, 17165 Stockholm, Sweden
[4]Department of Dermatology, Radboud University Medical Center, Nijmegen 6525GA, Güeldres, the Netherlands
[5]Department of Bioengineering and Centre for Synthetic Biology, Imperial College London, Greater London, London SW72AZ, UK
[6]These authors contributed equally
[7]Lead contact
*Correspondence: javier.santos@upf.edu (J.S.-M.), marc.guell@upf.edu (M.G.)
https://doi.org/10.1016/j.cels.2025.101169

## SUMMARY

Bacteria represent a promising dynamic delivery system for the treatment of disease. In the skin, the relevant location of *Cutibacterium acnes* within the hair follicle makes this bacterium an attractive chassis for dermal biotechnological applications. Here, we provide a genetic toolbox for the engineering of this traditionally intractable bacterium, including basic gene expression tools, biocontainment strategies, markerless genetic engineering, and dynamic transcriptional regulation. As a proof of concept, we develop an antioxidant-secreting strain capable of reducing oxidative stress in a UV stress model.

## INTRODUCTION

The skin is the largest organ in the human body. Beyond its function as a barrier against pathogens or environmental factors, the skin holds relevant physiological functions such as heat regulation or immune surveillance. At the same time, it represents a crucial determinant of our physical appearance and social contact.[1] More than 3,000 different conditions affect the skin, with almost one third of the world's population having at least one.[2,3] These diseases have a profound impact on patients' quality of life, ranging from life-threatening (malignant melanoma) to chronic and socially impairing conditions (psoriasis, atopic dermatitis [AD], or acne).[3] Environmental factors also influence skin health. For instance, excessive UV exposure causes premature aging and skin cancer.[4] Current treatments against the most frequent chronic skin conditions such as AD or psoriasis focus on symptom control and often cause side effects.[5,6] Novel treatments that target the underlying immune components of these diseases are effective, but they pose an economic burden on national healthcare systems[7]—e.g., dupilumab, a monoclonal antibody used for AD that blocks interleukin (IL)-4 and IL-13, has a yearly cost of more than $30,000 per patient.[8]

Engineered live biotherapeutic products (eLBPs) aim to combine the natural adaptation of human microbes to their host[9] with the synthetic design of sensors, circuits, and actuators that enhance the capabilities of those microbes. Although some eLBPs have already shown encouraging results in treating metabolic diseases,[10,11] infections,[12] or cancer[13] in the gut or even the lung,[14,15] there are still few instances of skin eLBPs. The most promising examples focus on engineering lactic acid bacteria or *Staphylococcus epidermidis* (*S. epidermidis*) for accelerated wound healing[16] or as cancer vaccines[17] and mosquito repellent,[18] with promising preliminary results in mice. These bacteria might produce transient benefits but are suboptimal as a long-term skin-resident eLBP. Lactic acid bacteria are not native skin residents, and their engraftment is low. Despite being ubiquitous in the skin, *S. epidermidis* shows a lower relative abundance and a higher turnover compared with other skin microbes like *Cutibacterium acnes* (*C. acnes*)[19]and might incur in horizontal gene transfer with related pathogens like *Staphylococcus aureus*.[20]

*C. acnes* is the most abundant skin commensal.[21] This gram-positive and facultative anaerobic bacterium predominantly colonizes the pilosebaceous units, where it metabolizes sebum lipids.[22] This specialized ecological niche constitutes a privileged location for eLBP deployment. The hair follicle is a physiological hotspot relevant for immune education and the main route for topical absorption of therapeutics.[23] The turnover of *C. acnes* in the skin is low,[19] and genomic studies report virtually monoclonal populations within pilosebaceous units,[24] with high genome stability across strains[25]; the low competition and low recombination events are relevant features regarding biosafety.[26] Although *C. acnes* has been historically associated with acne vulgaris, the overabundance of *C. acnes* does not adequately describe acne pathogenesis. Particular phylotypes—principally type IA1 strains—are associated strongly with this disease, whereas others—such as II or III—correlate with healthy skin.[27] In fact, some skin diseases such as AD

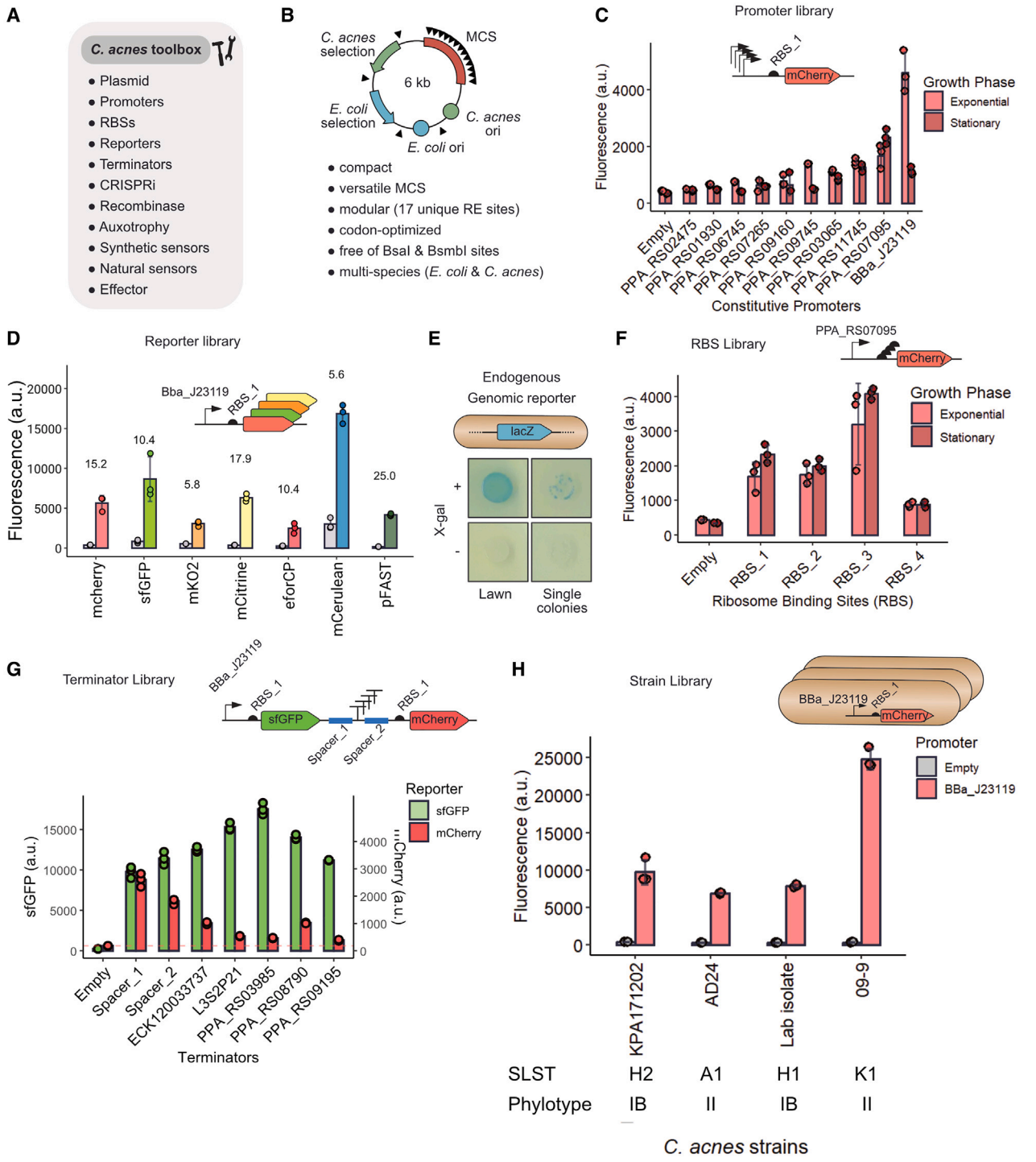


**Figure 1. Development of a toolbox for *C. acnes* genetic engineering**

(A) List of all tools developed in this study.

(B) Schematics of *C. acnes* replicative plasmid optimizations.

(C) Average of population median mCherry fluorescent values of three independent replicates for nine different constitutive endogenous promoters, a synthetic consensus promoter (BBa_J23119) from *E. coli*, and a control harboring a no-insert plasmid (Empty) for exponential and stationary growth phases.

(D) Average of population median fluorescent values for *C. acnes* harboring a fluorescent reporter (colored bars) compared with a no-insert plasmid control (gray bars). Values depicted above bars indicate average fold change of three independent replicates.

(E) Pictures representative of the *C. acnes* KPA171202 wild-type strain grown either as a lawn or as single colonies in a Brucella media agar plate, supplemented or not with X-gal.

*(legend continued on next page)*

generally show a characteristic decrease in *C. acnes* proportion in the skin.[28] In addition, *C. acnes* can be transplanted from donor to recipient skin using topical applications, which has been shown to modulate the relative abundance of recipient *C. acnes* strains for up to several weeks after an application of $10^6$ bacteria embedded in a gel for 3 consecutive days.[29,30] Taken together, *C. acnes* is an ideal chassis for skin eLBP development due to its location, high abundance, relevance in healthy skin, colonization capabilities, and low turnover, as we demonstrated recently through a sebum modulation application.[31]

In the present study, we establish an enabling toolbox for the traditionally intractable *C. acnes* to promote the development of microbiome-based skin therapies (Figure 1A). We demonstrate the use of these tools to discover auxotrophies and to create an antibiotic-marker-free strain for safe deployment in the skin. Moreover, we design a set of natural and synthetic inducible systems for the exogenous or environmental activation of gene expression. As a proof of concept for potential therapeutic applications, we create an antioxidant-producing strain able to rescue keratinocytes from UV-induced oxidative stress.

## RESULTS AND DISCUSSION

To construct this toolbox, we optimized a plasmid from *Propionibacterium freudenreichii* previously described to replicate in *C. acnes*[31,35,36] (Figure 1B). First, we removed all non-essential sequences as well as many restriction sites commonly used in classical or Golden Gate cloning, reducing the total vector size by more than 2 kb. Additionally, we adapted the plasmid for a modular cloning scheme based on isothermal (Gibson) assembly that allows us to standardize all our genetic parts with common prefix and suffix sequences for quick and modular cloning.[37] We also standardized and codon-optimized two antibiotic resistance cassettes—based on the *ermE* gene from *Saccharopolyspora erythraea* and the *cmx* gene from *Corynebacterium glutamicum*—and used one or the other as the *C. acnes* selection marker. The plasmid backbone contains two origins of replication (one for *E. coli*, the other for *C. acnes*) and two resistance cassettes (one for each of the bacterial hosts). To facilitate the straightforward replacement of those components, we flanked them with unique restriction sites.

We wanted to develop a collection of genetic parts enabling us and others to control and program the behavior of *C. acnes*. To this goal, we first tested a set of nine endogenous constitutive promoters that we previously identified by RNA sequencing (RNA-seq) (see STAR Methods) spanning a wide range of expression levels, with most functioning in both exponential and stationary growth phases (Figures 1C and S1). We also tested a synthetic *E. coli* consensus promoter (BBa_J23119) because of its similarity to the *C. acnes* −10 consensus box.[38] Interestingly, this promoter yielded the highest expression among those tested, although its expression decayed in the stationary phase (Figures 1C and S1). We also observed that some promoters showed a bimodal distribution, with one of the populations displaying a fluorescent intensity similar to that of the negative control (Figure S1). We decided to report the median of the entire population for simplifying comparisons with unimodal samples (Figure S1).

We then used the BBa_J23119 synthetic promoter to validate the suitability of seven fluorescent proteins as *C. acnes* reporters, including the anaerobic fluorescent tag pFAST.[39] Using flow cytometry, we observed an increase in fluorescent signal for all reporters when compared with an empty-plasmid control in exponential phase (Figures 1D and S2). In this case, we observed a clear bimodal distribution, except for pFAST. Therefore, we decided to establish a threshold and calculate the median of the population with the highest fluorescence intensity for comparisons (Figure S2). We selected mCherry for subsequent experiments due to its dynamic range (Figure 1D), its reported suitability in anaerobic bacteria after 2 h of maturation in aerobic conditions,[40,41] and its lack of dependence on commercial ligands, unlike pFAST. We also validated the use of the endogenous copy of *lacZ*—encoding beta-galactosidase—as a genomic reporter in the presence of X-gal (Figures 1E and S3). We next tested the strength of four different ribosome-binding sites (RBS): two of these (RBS_3 and RBS_4) were designed using the RBS calculator,[32] whereas the other two (RBS_1 and RBS_2) were strong RBS sequences from *E. coli*—indeed, the rRNA stretch that recognizes the Shine-Dalgarno sequence is only one nucleotide different between *C. acnes* and *E. coli* (Figures 1F and S4). We next measured the transcriptional termination of five sequences: two strong terminators reported to work in *E. coli* (a natural one and a synthetic one)[42] and three *C. acnes* endogenous sequences selected from RNA-seq. We used a dual reporter system where sfGFP and mCherry were transcribed together but are separated by the evaluated terminator sequence (Figure 1G). All five terminators yielded mCherry levels that were reduced with respect to non-terminator spacer controls and revealed terminator efficiencies ranging from 70% to 90% compared with the Spacer_1 control (Figures 1G, S5, and S6).

Human adults have a unique mixture of *C. acnes* strains.[21] Ideally, the engineering of different *C. acnes* strains could enable strain-specific eLBPs tailored to the patient's unique microbial

(F) Average of population median mCherry fluorescent values of three independent replicates for four different RBSs driving mCherry translation when expressed with the constitutive promoter PPA_RS07095, compared with a no-insert plasmid control (Empty) for exponential and stationary growth phases. RBS_1 and RBS_2 correspond to strong *E. coli* RBSs with the conserved AGGAGG motif, whereas RBS_3 and RBS_4 are *de novo* RBSs designed with the RBS calculator.[32]
(G) Average of population median mCherry (red) and sfGFP (green) fluorescent values of three independent replicates for five different transcriptional terminator sequences: the natural *E. coli* terminator ECK120033737, the synthetic terminator L3S2P21, and three endogenous terminator sequences from *C. acnes*. sfGFP and mCherry are located in the same transcriptional unit and the terminator is placed in-between. The whole transcriptional unit is expressed using the BBa_J23119 promoter and values are compared with a strain harboring a no-insert plasmid control (Empty) and two control strains with spacer sequences (Spacer_1 or Spacer_2) but no terminator. The red dashed line indicates the mCherry fluorescent value for the no-insert plasmid control (Empty).
(H) Average of population median mCherry fluorescent values of three independent replicates for four different *C. acnes* strains expressing mCherry controlled with the BBa_J23119 constitutive promoter (red), compared with the same strain harboring a no-insert plasmid (Empty, gray). The table below indicates the *C. acnes* sequence locus sequence typing (SLST)[33] or the recA-based phylotype[34] for each of the strains.

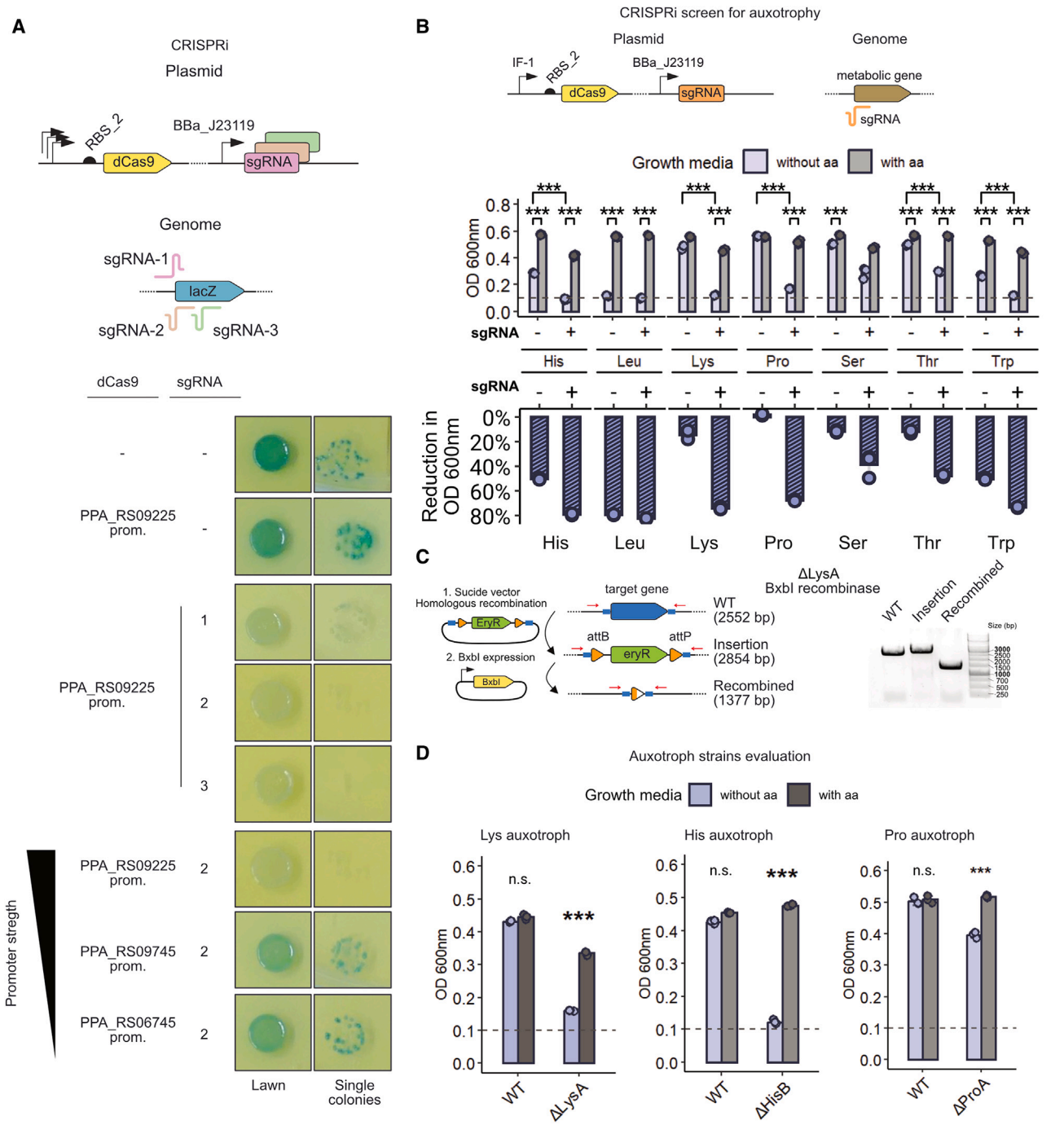


**Figure 2. CRISPR interference for quick prototyping of auxotrophies for biocontainment**

(A) dCas9 and gRNA optimization against the genomic reporter *lacZ* (PPA_RS08600). Pictures show the absence or presence of blue color in a representative *C. acnes* lawn or single colonies grown in Brucella media agar plates supplemented with X-gal.

(B) CRISPRi screen of *C. acnes* metabolic genes potentially leading to a single-gene knockout amino acid auxotrophy based on homology. Optical density at 600 nm ($OD_{600}$) of *C. acnes* cultures grown for 1 day in the presence or absence of a specific amino acid, compared with a control (dCas9) without gRNA cassette (i.e., without gRNA and its corresponding promoter). For instance, to evaluate His auxotrophy, the basal medium was supplemented with all amino acids except histidine and growth was measured both in the absence and presence of histidine for the auxotroph and dCas9 control. The dashed gray line indicates the starting culture $OD_{600}$ at 0.1. Statistical significance was determined using a Student's t test to compare (i) between the strains grown in the presence and absence of the studied amino acid or (ii) between the knockdown strain and the gRNA-lacking control, both grown with amino acid supplementation. A $p$ value < 0.001 is denoted with three stars (***). The graph below represents the percentage of $OD_{600}$ reduction of each strain grown in the absence of amino acid compared with the supplemented amino acid condition.

*(legend continued on next page)*

profile, therefore increasing engraftment. For this reason, we wondered how suitable our optimized plasmid and molecular tools were for other *C. acnes* strains spanning across two phylotypes[34] and four different sequence locus sequence typing (SLST) types.[33] All tested strains were able to incorporate our optimized plasmid and to express mCherry controlled by the BBa_J23119 synthetic promoter in exponential phase (Figures1H and S7). The fluorescent population in strain 09-9 was ~2.5-fold more fluorescent compared with the other strains. Interestingly, 09-9 harbors a native plasmid, including a putative *tad* locus hypothesized to be involved in plasmid transference.[43] This plasmid might be having a direct or indirect effect in the copy number of our engineered plasmid, thus affecting mCherry expression. However, other unknown effects such as differential promoter efficiencies across strains might also be involved in this observation.

Then, we used our basic genetic parts to further develop more advanced tools. To interrogate the function of endogenous genes, we sought to validate the use of CRISPR interference (CRISPRi) in *C. acnes*. We had observed that *C. acnes* is naturally able to degrade the synthetic compound X-gal to yield blue-colored colonies (Figure 1E), and we hypothesized that this β-galactosidase activity was due to a genomic *lacZ* homolog, PPA_RS08600. We designed single-guide RNAs (sgRNAs) against the 5′ end of the *lacZ* coding sequence, and we combined them with different expression levels of dCas9. Designs featuring high expression levels of dCas9 yielded colorless colonies in the presence of X-gal regardless of the sgRNA used, indicating an efficient repression of endogenous *lacZ* (Figures 2A and S8).

Next, we focused on designing a biocontainment strategy for *C. acnes* that ensures the safe deployment of therapeutically relevant strains. Our goal was to generate an auxotrophic strain without any heterologous antibiotic resistance gene. In view of the low genome integration efficiency in *C. acnes*,[31] we first tested the use of Cas9 as a way to screen for genes that would render *C. acnes* auxotrophic upon disruption. However, genome targeting by Cas9 seemed to be toxic for *C. acnes*—which is generally the case for bacteria due to non-repaired double-stranded breaks[44]—as suggested by the lack of transformants. Lowering the expression of Cas9 through the use of weaker promoters yielded transformants, but they lacked any edit in the genome. We then turned to plasmid-borne CRISPRi as a non-lethal approach to screen for genes that would yield auxotrophic *C. acnes* strains upon knockout. We targeted eight different putative gene candidates whose individual disruption would lead to an amino acid auxotrophy (Figure 2B), based on their homology to auxotrophic strains described in the *E. coli* KEIO collection.[45] We then evaluated which of the CRISPRi knockdowns impaired bacterial growth when the amino acid was not supplied in a rich defined custom medium (see STAR Methods). Lysine and proline biosynthesis pathway repression showed the highest growth defect compared with a dCas9-only control (Figure 2B). Histidine, leucine, and tryptophan pathway repression also showed growth defects, but growth was also reduced in the dCas9-only control, suggesting that the wild-type expression of the targeted genes cannot compensate for the absence of those amino acids in the medium (Figure 2B). Interestingly, we did not manage to knock down the cysteine pathway, likely due to the relevance of this amino acid for *C. acnes*.[46]

In the light of these results, we generated *C. acnes ΔlysA, ΔproA*, and *ΔhisB* strains by using a homologous recombination cassette harboring the erythromycin resistance gene *ermE* (Figures 2C and S8). To enable the removal of the genome-integrated antibiotic resistance gene, we flanked *ermE* with the *attP* and *attB* recombination sites specific for the BxbI serine integrase. Constitutive expression of the BxbI gene from a replicative plasmid selected with a different antibiotic resistance marker (*cmx*) resulted in the successful removal of the complete *ermE* gene for all tested colonies after transformation (Figures 2C, S9, and S10). After plasmid curation, we obtained three strains without any heterologous antibiotic resistance that preserved the corresponding gene deletions. As expected, the lack of *lysA* and *hisB* was enough to impair the growth of *C. acnes* after 4 days of incubation in the absence of lysine or histidine, respectively (Figures 2D and S11). In the case of histidine absence, the wild type had reduced growth after 24 h, as observed previously in the CRISPRi screening, but achieved a similar growth level to the histidine-supplemented culture after 4 days of growth, in contrast to the *ΔhisB* strain (Figures 2D and S11). We observed a similar behavior for lysine supplementation, where the wild type experienced a slower growth but recovered within 4 days, whereas the *ΔlysA* strain did not show any growth during that time. Regarding the proline auxotroph, *proA* deletion did not fully suppress growth but yielded a growth delay in the absence of proline that might impact its ability to compete with other skin-resident microbes and therefore be enough for biocontainment within the natural niche—the human skin (Figures 2D and S11). Although the concentration of free Lys, His, and Pro in corneocytes appears to be low on the skin surface,[47] a more biologically relevant and tissue realistic skin model is needed to further evaluate the performance of these auxotrophies as a real-world biocontainment strategy.

One of the key benefits of eLBPs is their ability to detect host or environmental signals and to dynamically produce relevant molecules with therapeutic potential. To build such a dynamic "smart" probiotic, we engineered different transcriptional sensors in *C. acnes* following two main strategies: the transplantation of known transcription factors (TFs) from other organisms and the *de novo* discovery of natural genetic resources from *C. acnes*. For the first approach, we decided to focus on two well-known repressors commonly used in model bacteria, TetR and PhlF. We designed different inducible promoters by placing one or more operator sequences (*tetO* or *phlO*) upstream, downstream, or

(C) Agarose gel showing the PCR amplification of the *lysA* locus from a wild-type strain (WT), a strain with an erythromycin cassette insertion flanked by BxbI recombination sites (Insertion), and a third strain in which the erythromycin cassette has been removed through BxbI expression (Recombined). The diagram shows the process to obtain such as a strain and the expected size for each locus amplification.
(D) Growth of a *ΔlysA, ΔproA,* and *ΔhisB* knockout strains compared with WT *C. acnes* in the presence or absence of L-lysine, L-proline, or L-histidine after 4 days of incubation. The dashed gray line indicates the starting culture $OD_{600}$ 0.1. Statistical significance was determined using a Student's t test to compare the strain when grown in the presence and absence of the studied amino acid. A $p$ value < 0.001 is denoted with three stars (***) and with ns when not significant.

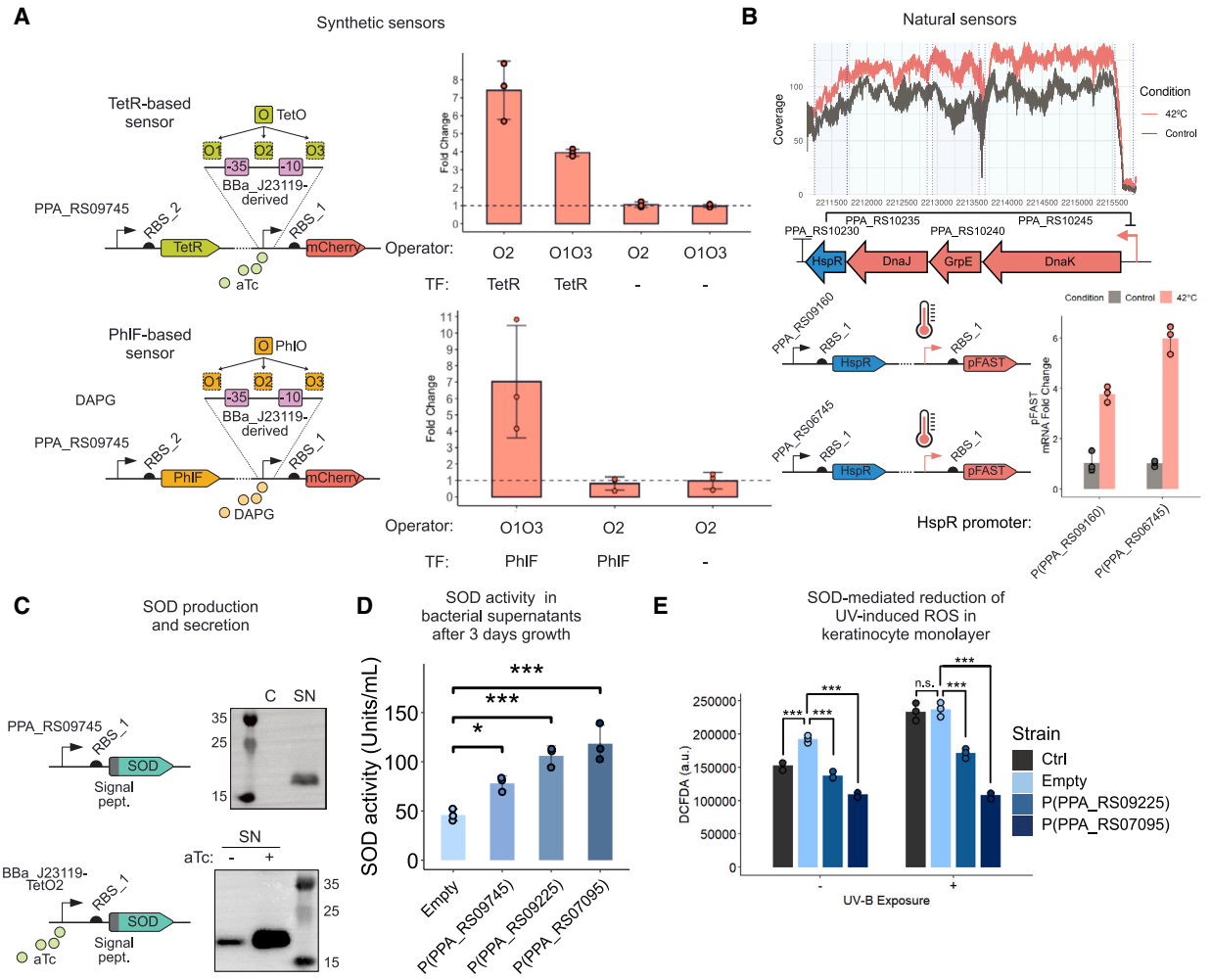


**Figure 3. Engineered sensing and actuation in *C. acnes***

(A) Schematics of synthetic BBa_J23119-based promoters, including operator sequences from the TetR and PhlF transcriptional repressors (left). Fold-change mCherry population median fluorescence upon induction, for different promoter architectures, in the presence or absence of the corresponding transcription factor (right).

(B) Adaptation of temperature-responsive *C. acnes* endogenous genes for temperature sensing. The graph on top displays the coverage of RNA-seq reads for a specific genome region containing the differentially expressed temperature-responsive operon. The diagrams depict the plasmid design of two temperature-sensing plasmids, both carrying the temperature-sensitive HspR transcription factor regulated by two distinct constitutive promoters (PPA_RS09160 and PPA_RS06745, respectively), alongside the temperature-responsive promoter controlling the pFAST reporter. The graph on the bottom right displays the average mRNA fold change increase in these two temperature-sensing strains upon 42°C heat-shock treatment measured by RT-qPCR.

(C) Top: western blot detection of SodC-F1 constitutively produced and secreted to the supernatant (labeled as SN) by an engineered *C. acnes* strain, compared with the cellular (labeled as C) fraction of the same strain. Bottom: western blot detection of aTc-inducible SodC-F1 production. Shown are supernatant (SN) fractions of uninduced (−) and induced (+) cultures.

(D) Superoxide dismutase activity measured in the supernatant of three different SodC-F1-producing strains with different constitutive promoter strengths (P(PPA_RS09745), P(PPA_RS09225) and P(PPA_RS07095)) compared with a no-insert plasmid control (Empty). Statistical significance was determined using a Student's t test to compare the SOD activity produced per strain. A $p$ value < 0.001 is denoted with three stars (***), < 0.01 with one star (*), and with ns if not significant.

(E) Reactive oxygen species (ROS) levels measured with CM-H2DCFDA fluorescent dye for N/TERT-2G keratinocytes cells exposed or not to UVB light. Cells were treated with media (Ctrl), with the supernatant of strains producing SodC-F1 constitutively (from P(PPA_RS09225) or P(PPA_RS07095) promoters), or with the supernatant of a no-insert plasmid control (Empty). Statistical significance was determined using an ANOVA to compare the ROS levels between samples. A $p$ value < 0.001 is denoted with three stars (***) and with ns if not significant.

between the −35 and −10 boxes of BBa_ J23119, and we combined the resulting promoters with different expression levels of the corresponding TFs (Figure 3A). In the presence of the inducer (aTc for TetR, DAPG for PhlF), some of the designs yielded inducible mCherry expression of up to ~7-fold compared with the non-induced control (Figures 3A, S12, and S13). Although sensors in model bacteria can display large dynamic ranges (of up to three or four orders of magnitude in some cases) as a result of

numerous optimizations throughout years of research, the fold induction of TFs used in non-model bacteria is generally more modest, often in the range of one order of magnitude[48]—e.g., 10-fold for GlnR in *Pseudomonas putida*,[49] 7-fold for FNR in *Synechocystis* sp. PCC 6803,[50] or 5-fold for AceT in *Rhodococcus opacus*.[51]

To discover and co-opt the natural TFs already present in the *C. acnes* genome, we performed an RNA-seq on *C. acnes* upon temperature shock, which represents an environmental signal with potential relevance in the skin context. Indeed, temperature-change detection has been previously used to trigger the self-destruction of bacteria leaving the body (i.e., kill switch) for biocontainment,[52] or as an activation mechanism induced by ultrasounds.[53] We exposed *C. acnes* to a 42°C heat shock for 15 min and we looked for upregulated genes with RNA-seq. From hidden Markov models (HMMs) and operon structure conservation, we identified a conserved DnaK-GrpE-DnaJ-HspR chaperon operon well-known in other bacteria to regulate protein refolding in heat-shock stress (Figure 3B). Specifically, the HspR transcriptional regulator is involved in the regulation of the operon,[54,55] and we thus cloned the regulatory sequence together with the constitutively expressed HspR in our replicative plasmid. We tested two plasmid constructs differing only in the strength of the constitutive promoter used to express HspR (Figure 3B). We measured the pFAST reporter mRNA expression by RT-qPCR after a 42°C heat shock and observed a 4- and 6-fold increase at the mRNA levels, respectively (Figure 3B). The higher fold change observed when HspR is expressed from the P(PPA_RS06745) promoter is likely due to the greater abundance of the repressor due to the strength of this constitutive promoter. Typically, higher repressor concentrations decrease basal expression levels and result in a greater change in expression upon induction.[56]

Ideally, eLBPs should have the dual ability to not only sense the environment but also produce proteins or molecules with therapeutic relevance directly on the appropriate biological niche. Chronic inflammation and excessive UV exposure lead to prolonged reactive oxygen species (ROS) release, eventually damaging the skin structure and physiology.[4,57] We therefore engineered an antioxidant-secreting *C. acnes* strain for reducing oxidative stress. Superoxide dismutases (SODs) are enzymes that neutralize the superoxide anion ($O_2^-$) and protect cells from oxidative damage. Among these enzymes, the SodC-F1 from the enterohemorrhagic *E. coli* O157:H7 has shown to be functional in the periplasm, stable against proteases, and exhibit high catalytic activity, representing one of the principal defense mechanisms of this bacterium against ROS.[58] We hypothesized that expressing this enzyme in *C. acnes* could reduce ROS levels. To prove this, we first coupled the enzyme with a secretion signal from a highly secreted endogenous protein, RoxP.[59,60] Indeed, the protein was correctly produced and secreted (Figures 3C and S14), and it maintained its SOD activity in the supernatant (Figure 3D). We also demonstrated the usefulness of our newly developed transcriptional sensors by constructing a strain that produces and secretes SodC-F1 in an aTc-inducible manner (Figures 3C and S15). We next challenged the immortalized keratinocyte cell line N/TERT-2G[61,62] with UVB to induce the formation of ROS. Thereafter, we treated the cells with *C. acnes* supernatants and quantified ROS levels using the fluorescent dye CM-H2DCFDA. The SodC-F1 produced by *C. acnes* was able to significantly reduce UV-mediated ROS levels in keratinocytes (Figure 3E). The reduction correlated with the strength of the promoter regulating SodC-F1 expression, suggesting that we would be able to adjust the antioxidant activity of the engineered strain to match the requirements of the final application. Yet, a more realistic skin model would be needed to evaluate the advantages of using a living engineered commensal compared with simple recombinant protein application. Moreover, future deployments of this antioxidant eLBP could incorporate inducible SOD expression, either through artificial inducers like aTc (Figures 3C and S15) or in response to environmental triggers such as UV-damage markers produced by keratinocytes. For instance, a bacterial ROS sensor (such as OxyR[63]) controlling the expression of SOD depending on the ROS produced by keratinocytes upon UV exposure would result in an adaptative antioxidant eLBP.

In conclusion, we have established *C. acnes* as an amenable chassis for eLBPs development with potential applications in the skin. We describe a versatile toolbox for its engineering, as well as an auxotrophic strain, and antibiotic-free methodologies for genetic engineering toward its safe application in the skin. We demonstrate the detection of both artificial and environmental cues by engineered *C. acnes*, and we provide a proof-of-concept demonstration of oxidative stress reduction on keratinocytes. Taken together, our results pave the way for the use of *C. acnes* for microbiome-based skin therapies. Finally, all these tools are available for the research community to accelerate skin microbiome research using the most abundant skin commensal.

## RESOURCE AVAILABILITY

### Lead contact

Further information and requests for resources and reagents should be directed to and will be fulfilled by the lead contact, Marc Güell (marc.guell@upf.edu).

### Materials availability

Plasmids used in this study are listed in Table S3, and all sequences are provided in Data S1. Relevant plasmids will be available through Addgene (Addgene: 84704) and the Standard European Vector Architecture (SEVA) sibling collection.

### Data and code availability

- All RNA-seq reads will be available in the European Nucleotide Archive (ENA) repository under the PRJEB78978 project accession (ENA: PRJEB78978). Original western blot images are provided in the supplemental information (Figures S14 and S15). All other data reported in this paper will be shared by the lead contact upon request.
- This paper does not report original code. Custom scripts were only used for plotting the figures. These custom scripts for analysis and plotting are available in the following Zenodo repository: https://doi.org/10.5281/zenodo.14346074.
- Any additional information required to reanalyze the data reported in this paper is available from the lead contact upon request.

## ACKNOWLEDGMENTS

The authors thank master's students Marta Fa, Patricia Tresguerres, Anastasiya Petrenko, Carmen Argilés Rodríguez, and Saptashwa Datta and bachelor's students Lucía López Alcaide, Roger Torra Vaquero, and Zeynep Yeni for their technical assistance during their research internships. In addition,

we would like to thank Cristina Fernandez for her support and technical assistance. We would also like to thank Dr. Holger Brüggemann and Dr. Rolf Lood for kindly providing the AD24 and 09-9 *C. acnes* strains, respectively. This project was funded by SKINDEV "Skin microbial devices" by the European Innovation Council (EIC Pathfinder) (grant agreement no. 101098826) and the Office of Naval Research (award N62909-18-1-2155). J.S.-M. was funded by a Marie Skłodowska-Curie Individual Fellowship (European Union's Horizon 2020 Research and Innovation Programme under Marie Skłodowska-Curie grant agreement 882387), a Juan de la Cierva Incorporación Fellowship (grant no. IJC2020-043621-I funded by MICIU/AEI/10.13039/501100011033 and by European Union NextGenerationEU/PRTR), and a DCEXS MM postdoctoral project (Unidad de Excelencia María de Maeztu, funded by the AEI, ref. no. CEX2018-000792-M). G.N. was funded by an FI Fellowship (AGAUR-Catalan Government) co-funded by the European Social Fund (award 2020 FI-B 00107).

## AUTHOR CONTRIBUTIONS

G.N., J.S.-M., and M.G. designed the research. G.N., J.S.-M., and M.G. drafted the initial manuscript. G.N., with the help of J.S.-M., performed the CRISPRi auxotrophy screen and created the promoter, RBS, reporter, and auxotrophic and temperature-sensing strains. J.S.-M., with the help of G.N., established the CRISPRi methodology, standardized the expression vector, and created the chemically inducible and antioxidant strains. C.P.-C., with the help of J.S.-M. and G.N., constructed and assessed the aTc-inducible antioxidant strain. G.N., with the help of J.S.-M. and the guidance of E.H.v.d.B. and P.A.M.J., evaluated the antioxidant properties in the UV cell models. L.T. helped in all the above experimental procedures. I.B., with the help of G.N., J.S.-M., and R.L.-A., established the terminator strains. G.N., with the help of N.C.-S., performed the RNA-seq experiments, and N.C.-S. established the RNA-seq analysis pipeline. E.H.v.d.B. and P.A.M.J. provided the N/TERT-2G keratinocyte cell line and guided experiments with the keratinocytes. All authors read, edited, and approved the final manuscript.

## DECLARATION OF INTERESTS

M.G., J.S.-M., and G.N. filed patents in some of the technologies described in the manuscript. J.S.-M. declares having collaborated with Fundación de Ciencias de la Salud for scientific outreach activities.

## STAR★METHODS

Detailed methods are provided in the online version of this paper and include the following:

- KEY RESOURCES TABLE
- EXPERIMENTAL MODEL AND STUDY PARTICIPANT DETAILS
  - Microbial strains and media
- METHOD DETAILS
  - Plasmids and molecular biology
  - *C. acnes* electrocompetent cell preparation and transformation
  - Immunodetection of secreted SOD
  - N/TERT-2G cell culture, UV-exposure and AD monolayer model
  - RNA extraction
  - RT-qPCR
  - Homology search
- QUANTIFICATION AND STATISTICAL ANALYSIS
  - Flow cytometry
  - RNA-seq
  - SOD activity quantification
  - Statistics and reproducibility

## SUPPLEMENTAL INFORMATION

Supplemental information can be found online at https://doi.org/10.1016/j.cels.2025.101169.

Received: April 28, 2024
Revised: September 3, 2024
Accepted: January 9, 2025
Published: February 6, 2025

## REFERENCES

1. Hay, R.J., Augustin, M., Griffiths, C.E.M., and Sterry, W.; Board of the International League of Dermatological Societies and the Grand Challenges Consultation groups (2015). The global challenge for skin health. Br. J. Dermatol. *172*, 1469–1472. https://doi.org/10.1111/bjd.13854.
2. Hay, R.J., Johns, N.E., Williams, H.C., Bolliger, I.W., Dellavalle, R.P., Margolis, D.J., Marks, R., Naldi, L., Weinstock, M.A., Wulf, S.K., et al. (2014). The global burden of skin disease in 2010: an analysis of the prevalence and impact of skin conditions. J. Invest. Dermatol. *134*, 1527–1534. https://doi.org/10.1038/jid.2013.446.
3. Richard, M.A., Paul, C., Nijsten, T., Gisondi, P., Salavastru, C., Taieb, C., Trakatelli, M., Puig, L., and Stratigos, A.; EADV burden of skin diseases project team (2022). Prevalence of most common skin diseases in Europe: a population-based study. J. Eur. Acad. Dermatol. Venereol. *36*, 1088–1096. https://doi.org/10.1111/jdv.18050.
4. Quan, T. (2023). Molecular insights of human skin epidermal and dermal aging. J. Dermatol. Sci. *112*, 48–53. https://doi.org/10.1016/j.jdermsci.2023.08.006.
5. Nikam, R.V., Gowtham, M., More, P.S., and Shinde, A.S. (2023). Current and emerging prospects in the psoriatic treatment. Int. Immunopharmacol. *120*, 110331. https://doi.org/10.1016/j.intimp.2023.110331.
6. Sesi, J., and Feldman, S.R. (2024). Comparative efficacy of systemic treatments for atopic dermatitis in adults. Expert Rev. Clin. Immunol. *20*, 313–320. https://doi.org/10.1080/1744666X.2023.2291038.
7. Heinz, K.C., Beaudart, C., Willems, D., Wiethoff, I., and Hiligsmann, M. (2023). Cost-Effectiveness of Emerging Treatments for Atopic Dermatitis: A Systematic Review. Pharmacoeconomics *41*, 1415–1435. https://doi.org/10.1007/s40273-023-01293-4.
8. Zimmermann, M., Rind, D., Chapman, R., Kumar, V., Kahn, S., and Carlson, J. (2018). Economic Evaluation of Dupilumab for Moderate-to-Severe Atopic Dermatitis: A Cost-Utility Analysis. J. Drugs Dermatol. *17*, 750–756.
9. Isabella, V.M., Ha, B.N., Castillo, M.J., Lubkowicz, D.J., Rowe, S.E., Millet, Y.A., Anderson, C.L., Li, N., Fisher, A.B., West, K.A., et al. (2018). Development of a synthetic live bacterial therapeutic for the human metabolic disease phenylketonuria. Nat. Biotechnol. *36*, 857–864. https://doi.org/10.1038/nbt.4222.
10. Puurunen, M.K., Vockley, J., Searle, S.L., Sacharow, S.J., Phillips, J.A., 3rd, Denney, W.S., Goodlett, B.D., Wagner, D.A., Blankstein, L., Castillo, M.J., et al. (2021). Safety and pharmacodynamics of an engineered E. coli Nissle for the treatment of phenylketonuria: a first-in-human phase 1/2a study. Nat. Metab. *3*, 1125–1132. https://doi.org/10.1038/s42255-021-00430-7.
11. Lubkowicz, D., Horvath, N.G., James, M.J., Cantarella, P., Renaud, L., Bergeron, C.G., Shmueli, R.B., Anderson, C., Gao, J.-R., Kurtz, C.B., et al. (2022). An engineered bacterial therapeutic lowers urinary oxalate in preclinical models and in silico simulations of enteric hyperoxaluria. Mol. Syst. Biol. *18*, e10539. https://doi.org/10.15252/msb.202110539.
12. Mao, N., Cubillos-Ruiz, A., Cameron, D.E., and Collins, J.J. (2018). Probiotic strains detect and suppress cholera in mice. Sci. Transl. Med. *10*, eaao2586. https://doi.org/10.1126/scitranslmed.aao2586.
13. Leventhal, D.S., Sokolovska, A., Li, N., Plescia, C., Kolodziej, S.A., Gallant, C.W., Christmas, R., Gao, J.-R., James, M.J., Abin-Fuentes, A., et al. (2020). Immunotherapy with engineered bacteria by targeting the STING pathway for anti-tumor immunity. Nat. Commun. *11*, 2739. https://doi.org/10.1038/s41467-020-16602-0.
14. Mazzolini, R., Rodríguez-Arce, I., Fernández-Barat, L., Piñero-Lambea, C., Garrido, V., Rebollada-Merino, A., Motos, A., Torres, A., Grilló, M.J.,

Serrano, L., et al. (2023). Engineered live bacteria suppress Pseudomonas aeruginosa infection in mouse lung and dissolve endotracheal-tube biofilms. Nat. Biotechnol. *41*, 1089–1098. https://doi.org/10.1038/s41587-022-01584-9.

15. Montero-Blay, A., Blanco, J.D., Rodriguez-Arce, I., Lastrucci, C., Piñero-Lambea, C., Lluch-Senar, M., and Serrano, L. (2023). Bacterial expression of a designed single-chain IL-10 prevents severe lung inflammation. Mol. Syst. Biol. *19*, e11037. https://doi.org/10.15252/msb.202211037.
16. Öhnstedt, E., Vågesjö, E., Fasth, A., Lofton Tomenius, H., Dahg, P., Jönsson, S., Tyagi, N., Åström, M., Myktybekova, Z., Ringstad, L., et al. (2023). Engineered bacteria to accelerate wound healing: an adaptive, randomised, double-blind, placebo-controlled, first-in-human phase 1 trial. eClinicalMedicine *60*, 102014. https://doi.org/10.1016/j.eclinm.2023.102014.
17. Chen, Y.E., Bousbaine, D., Veinbachs, A., Atabakhsh, K., Dimas, A., Yu, V.K., Zhao, A., Enright, N.J., Nagashima, K., Belkaid, Y., et al. (2023). Engineered skin bacteria induce antitumor T cell responses against melanoma. Science *380*, 203–210. https://doi.org/10.1126/science.abp9563.
18. Liu, F., Coutinho-Abreu, I.V., Raban, R., Nguyen, T.T.D., Dimas, A.R., Merriman, J.A., and Akbari, O.S. (2023). Engineered Skin Microbiome Reduces Mosquito Attraction to Mice. bioRxiv. https://doi.org/10.1101/2023.12.20.572663.
19. Oh, J., Byrd, A.L., Park, M., NISC Comparative Sequencing Program, Kong, H.H., and Segre, J.A. (2016). Temporal Stability of the Human Skin Microbiome. Cell *165*, 854–866. https://doi.org/10.1016/j.cell.2016.04.008.
20. Zhou, W., Spoto, M., Hardy, R., Guan, C., Fleming, E., Larson, P.J., Brown, J.S., and Oh, J. (2020). Host-Specific Evolutionary and Transmission Dynamics Shape the Functional Diversification of Staphylococcus epidermidis in Human Skin. Cell *180*, 454–470.e18. https://doi.org/10.1016/j.cell.2020.01.006.
21. Oh, J., Byrd, A.L., Deming, C., Conlan, S., NISC Comparative Sequencing Program, Kong, H.H., and Segre, J.A. (2014). Biogeography and individuality shape function in the human skin metagenome. Nature *514*, 59–64. https://doi.org/10.1038/nature13786.
22. Gribbon, E.M., Cunliffe, W.J., and Holland, K.T. (1993). Interaction of Propionibacterium acnes with skin lipids in vitro. J. Gen. Microbiol. *139*, 1745–1751. https://doi.org/10.1099/00221287-139-8-1745.
23. Barry, B.W. (2002). Drug delivery routes in skin: a novel approach. Adv. Drug Deliv. Rev. *54*, S31–S40. https://doi.org/10.1016/s0169-409x(02)00113-8.
24. Conwill, A., Kuan, A.C., Damerla, R., Poret, A.J., Baker, J.S., Tripp, A.D., Alm, E.J., and Lieberman, T.D. (2022). Anatomy promotes neutral coexistence of strains in the human skin microbiome. Cell Host Microbe *30*, 171–182.e7. https://doi.org/10.1016/j.chom.2021.12.007.
25. Scholz, C.F.P., Brüggemann, H., Lomholt, H.B., Tettelin, H., and Kilian, M. (2016). Genome stability of Propionibacterium acnes: a comprehensive study of indels and homopolymeric tracts. Sci. Rep. *6*, 20662. https://doi.org/10.1038/srep20662.
26. Moe-Behrens, G.H.G., Davis, R., and Haynes, K.A. (2013). Preparing synthetic biology for the world. Front. Microbiol. *4*, 5. https://doi.org/10.3389/fmicb.2013.00005.
27. Dreno, B., Dekio, I., Baldwin, H., Demessant, A.L., Dagnelie, M.-A., Khammari, A., and Corvec, S. (2024). Acne microbiome: From phyla to phylotypes. J. Eur. Acad. Dermatol. Venereol. *38*, 657–664. https://doi.org/10.1111/jdv.19540.
28. Koh, L.F., Ong, R.Y., and Common, J.E. (2022). Skin microbiome of atopic dermatitis. Allergol. Int. *71*, 31–39. https://doi.org/10.1016/j.alit.2021.11.001.
29. Paetzold, B., Willis, J.R., Pereira de Lima, J., Knödlseder, N., Brüggemann, H., Quist, S.R., Gabaldón, T., and Güell, M. (2019). Skin microbiome modulation induced by probiotic solutions. Microbiome *7*, 95. https://doi.org/10.1186/s40168-019-0709-3.
30. Karoglan, A., Paetzold, B., Pereira de Lima, J., Brüggemann, H., Tüting, T., Schanze, D., Güell, M., and Gollnick, H. (2019). Safety and Efficacy of Topically Applied Selected Cutibacterium acnes Strains over Five Weeks in Patients with Acne Vulgaris: An Open-label, Pilot Study. Acta Derm. Venereol. *99*, 1253–1257. https://doi.org/10.2340/00015555-3323.
31. Knödlseder, N., Fábrega, M.-J., Santos-Moreno, J., Manils, J., Toloza, L., Marín Vilar, M., Fernández, C., Broadbent, K., Maruotti, J., Lemenager, H., et al. (2024). Delivery of a sebum modulator by an engineered skin microbe in mice. Nat. Biotechnol. *42*, 1661–1666. https://doi.org/10.1038/s41587-023-02072-4.
32. Salis, H.M., Mirsky, E.A., and Voigt, C.A. (2009). Automated design of synthetic ribosome binding sites to control protein expression. Nat. Biotechnol. *27*, 946–950. https://doi.org/10.1038/nbt.1568.
33. Scholz, C.F.P., Jensen, A., Lomholt, H.B., Brüggemann, H., and Kilian, M. (2014). A Novel High-Resolution Single Locus Sequence Typing Scheme for Mixed Populations of Propionibacterium acnes In Vivo. PLoS One *9*, e104199. https://doi.org/10.1371/journal.pone.0104199.
34. Kilian, M., Scholz, C.F.P., and Lomholt, H.B. (2012). Multilocus Sequence Typing and Phylogenetic Analysis of Propionibacterium acnes. J. Clin. Microbiol. *50*, 1158–1165. https://doi.org/10.1128/JCM.r06129-11.
35. Lood, R. (2011). Propionibacterium acnes and its phages. PhD thesis (Lund University).
36. Jore, J.P., van Luijk, N., Luiten, R.G., van der Werf, M.J., and Pouwels, P.H. (2001). Efficient transformation system for Propionibacterium freudenreichii based on a novel vector. Appl. Environ. Microbiol. *67*, 499–503. https://doi.org/10.1128/AEM.67.2.499-503.2001.
37. Santos-Moreno, J., and Schaerli, Y. (2019). A Framework for the Modular and Combinatorial Assembly of Synthetic Gene Circuits. ACS Synth. Biol. *8*, 1691–1697. https://doi.org/10.1021/acssynbio.9b00174.
38. Lin, Y.F., A, D.R., Guan, S., Mamanova, L., and McDowall, K.J. (2013). A combination of improved differential and global RNA-seq reveals pervasive transcription initiation and events in all stages of the life-cycle of functional RNAs in Propionibacterium acnes, a major contributor to widespread human disease. BMC Genomics *14*, 620. https://doi.org/10.1186/1471-2164-14-620.
39. Benaissa, H., Ounoughi, K., Aujard, I., Fischer, E., Goïame, R., Nguyen, J., Tebo, A.G., Li, C., Le Saux, T., Bertolin, G., et al. (2021). Engineering of a fluorescent chemogenetic reporter with tunable color for advanced live-cell imaging. Nat. Commun. *12*, 6989. https://doi.org/10.1038/s41467-021-27334-0.
40. Pinilla-Redondo, R., Riber, L., and Sørensen, S.J. (2018). Fluorescence Recovery Allows the Implementation of a Fluorescence Reporter Gene Platform Applicable for the Detection and Quantification of Horizontal Gene Transfer in Anoxic Environments. Appl. Environ. Microbiol. *84*. e02507-17. https://doi.org/10.1128/AEM.02507-17.
41. Ransom, E.M., Ellermeier, C.D., and Weiss, D.S. (2015). Use of mCherry Red fluorescent protein for studies of protein localization and gene expression in Clostridium difficile. Appl. Environ. Microbiol. *81*, 1652–1660. https://doi.org/10.1128/AEM.03446-14.
42. Chen, Y.-J., Liu, P., Nielsen, A.A.K., Brophy, J.A.N., Clancy, K., Peterson, T., and Voigt, C.A. (2013). Characterization of 582 natural and synthetic terminators and quantification of their design constraints. Nat. Methods *10*, 659–664. https://doi.org/10.1038/nmeth.2515.
43. Davidsson, S., Carlsson, J., Mölling, P., Gashi, N., Andrén, O., Andersson, S.-O., Brzuszkiewicz, E., Poehlein, A., Al-Zeer, M.A., Brinkmann, V., et al. (2017). Prevalence of Flp Pili-Encoding Plasmids in Cutibacterium acnes Isolates Obtained from Prostatic Tissue. Front. Microbiol. *8*, 2241. https://doi.org/10.3389/fmicb.2017.02241.
44. Cui, L., and Bikard, D. (2016). Consequences of Cas9 cleavage in the chromosome of Escherichia coli. Nucleic Acids Res. *44*, 4243–4251. https://doi.org/10.1093/nar/gkw223.
45. Baba, T., Ara, T., Hasegawa, M., Takai, Y., Okumura, Y., Baba, M., Datsenko, K.A., Tomita, M., Wanner, B.L., and Mori, H. (2006). Construction of Escherichia coli K-12 in-frame, single-gene knockout

mutants: the Keio collection. Mol. Syst. Biol. *2*, 2006.0008. https://doi.org/10.1038/msb4100050.

46. Nielsen, P.A. (1983). Role of reduced sulfur compounds in nutrition of Propionibacterium acnes. J. Clin. Microbiol. *17*, 276–279. https://doi.org/10.1128/jcm.17.2.276-279.1983.
47. Mark, H., and Harding, C.R. (2013). Amino acid composition, including key derivatives of eccrine sweat: potential biomarkers of certain atopic skin conditions. Int. J. Cosmet. Sci. *35*, 163–168. https://doi.org/10.1111/ics.12019.
48. Kim, N.M., Sinnott, R.W., and Sandoval, N.R. (2020). Transcription factor-based biosensors and inducible systems in non-model bacteria: current progress and future directions. Curr. Opin. Biotechnol. *64*, 39–46. https://doi.org/10.1016/j.copbio.2019.09.009.
49. Xiao, Y., Jiang, W., and Zhang, F. (2017). Developing a Genetically Encoded, Cross-Species Biosensor for Detecting Ammonium and Regulating Biosynthesis of Cyanophycin. ACS Synth. Biol. *6*, 1807–1815. https://doi.org/10.1021/acssynbio.7b00069.
50. Immethun, C.M., Ng, K.M., DeLorenzo, D.M., Waldron-Feinstein, B., Lee, Y.-C., and Moon, T.S. (2016). Oxygen-responsive genetic circuits constructed in Synechocystis sp. PCC 6803. Biotechnol. Bioeng. *113*, 433–442. https://doi.org/10.1002/bit.25722.
51. DeLorenzo, D.M., Henson, W.R., and Moon, T.S. (2017). Development of Chemical and Metabolite Sensors for Rhodococcus opacus PD630. ACS Synth. Biol. *6*, 1973–1978. https://doi.org/10.1021/acssynbio.7b00192.
52. Rottinghaus, A.G., Ferreiro, A., Fishbein, S.R.S., Dantas, G., and Moon, T.S. (2022). Genetically stable CRISPR-based kill switches for engineered microbes. Nat. Commun. *13*, 672. https://doi.org/10.1038/s41467-022-28163-5.
53. Abedi, M.H., Yao, M.S., Mittelstein, D.R., Bar-Zion, A., Swift, M.B., Lee-Gosselin, A., Barturen-Larrea, P., Buss, M.T., and Shapiro, M.G. (2022). Ultrasound-controllable engineered bacteria for cancer immunotherapy. Nat. Commun. *13*, 1585. https://doi.org/10.1038/s41467-022-29065-2.
54. Das Gupta, T., Bandyopadhyay, B., and Das Gupta, S.K. (2008). Modulation of DNA-binding activity of Mycobacterium tuberculosis HspR by chaperones. Microbiology (Reading) *154*, 484–490. https://doi.org/10.1099/mic.0.2007/012294-0.
55. Spohn, G., and Scarlato, V. (1999). The autoregulatory HspR repressor protein governs chaperone gene transcription in Helicobacter pylori. Mol. Microbiol. *34*, 663–674. https://doi.org/10.1046/j.1365-2958.1999.01625.x.
56. Georgi, C., Buerger, J., Hillen, W., and Berens, C. (2012). Promoter strength driving TetR determines the regulatory properties of Tet-controlled expression systems. PLoS One *7*, e41620. https://doi.org/10.1371/journal.pone.0041620.
57. Wagener, F.A.D.T.G., Carels, C.E., and Lundvig, D.M.S. (2013). Targeting the Redox Balance in Inflammatory Skin Conditions. Int. J. Mol. Sci. *14*, 9126–9167. https://doi.org/10.3390/ijms14059126.
58. D'Orazio, M., Scotti, R., Nicolini, L., Cervoni, L., Rotilio, G., Battistoni, A., and Gabbianelli, R. (2008). Regulatory and structural properties differentiating the chromosomal and the bacteriophage-associated Escherichia coli O157:H7 Cu, Zn superoxide dismutases. BMC Microbiol. *8*, 166. https://doi.org/10.1186/1471-2180-8-166.
59. Holland, C., Mak, T.N., Zimny-Arndt, U., Schmid, M., Meyer, T.F., Jungblut, P.R., and Brüggemann, H. (2010). Proteomic identification of secreted proteins of Propionibacterium acnes. BMC Microbiol. *10*, 230. https://doi.org/10.1186/1471-2180-10-230.
60. Allhorn, M., Arve, S., Brüggemann, H., and Lood, R. (2016). A novel enzyme with antioxidant capacity produced by the ubiquitous skin colonizer Propionibacterium acnes. Sci. Rep. *6*, 36412. https://doi.org/10.1038/srep36412.
61. Smits, J.P.H., Niehues, H., Rikken, G., van Vlijmen-Willems, I.M.J.J., van de Zande, G.W.H.J.F., Zeeuwen, P.L.J.M., Schalkwijk, J., and van den Bogaard, E.H. (2017). Immortalized N/TERT keratinocytes as an alternative cell source in 3D human epidermal models. Sci. Rep. *7*, 11838. https://doi.org/10.1038/s41598-017-12041-y.
62. Dickson, M.A., Hahn, W.C., Ino, Y., Ronfard, V., Wu, J.Y., Weinberg, R.A., Louis, D.N., Li, F.P., and Rheinwald, J.G. (2000). Human keratinocytes that express hTERT and also bypass a p16(INK4a)-enforced mechanism that limits life span become immortal yet retain normal growth and differentiation characteristics. Mol. Cell. Biol. *20*, 1436–1447. https://doi.org/10.1128/MCB.20.4.1436-1447.2000.
63. Müller, I.E., Rubens, J.R., Jun, T., Graham, D., Xavier, R., and Lu, T.K. (2019). Gene networks that compensate for crosstalk with crosstalk. Nat. Commun. *10*, 4028. https://doi.org/10.1038/s41467-019-12021-y.
64. Lood, R., Mörgelin, M., Holmberg, A., Rasmussen, M., and Collin, M. (2008). Inducible Siphoviruses in superficial and deep tissue isolates of Propionibacterium acnes. BMC Microbiol. *8*, 139. https://doi.org/10.1186/1471-2180-8-139.
65. Hahne, F., LeMeur, N., Brinkman, R.R., Ellis, B., Haaland, P., Sarkar, D., Spidlen, J., Strain, E., and Gentleman, R. (2009). flowCore: a Bioconductor package for high throughput flow cytometry. BMC Bioinformatics *10*, 106. https://doi.org/10.1186/1471-2105-10-106.
66. Killick, R., and Eckley, I.A. (2014). Changepoint: An R Package for Changepoint Analysis. J. Stat. Softw. *58*, 1–19. https://doi.org/10.18637/jss.v058.i03.
67. Ewels, P.A., Peltzer, A., Fillinger, S., Patel, H., Alneberg, J., Wilm, A., Garcia, M.U., Di Tommaso, P., and Nahnsen, S. (2020). The nf-core framework for community-curated bioinformatics pipelines. Nat. Biotechnol. *38*, 276–278. https://doi.org/10.1038/s41587-020-0439-x.
68. Di Tommaso, P., Chatzou, M., Floden, E.W., Barja, P.P., Palumbo, E., and Notredame, C. (2017). Nextflow enables reproducible computational workflows. Nat. Biotechnol. *35*, 316–319. https://doi.org/10.1038/nbt.3820.
69. Dobin, A., Davis, C.A., Schlesinger, F., Drenkow, J., Zaleski, C., Jha, S., Batut, P., Chaisson, M., and Gingeras, T.R. (2013). STAR: ultrafast universal RNA-seq aligner. Bioinformatics *29*, 15–21. https://doi.org/10.1093/bioinformatics/bts635.
70. Li, H., Handsaker, B., Wysoker, A., Fennell, T., Ruan, J., Homer, N., Marth, G., Abecasis, G., and Durbin, R.; 1000 Genome Project Data Processing Subgroup (2009). The Sequence Alignment/Map format and SAMtools. Bioinformatics *25*, 2078–2079. https://doi.org/10.1093/bioinformatics/btp352.
71. Li, H. (2011). A statistical framework for SNP calling, mutation discovery, association mapping and population genetical parameter estimation from sequencing data. Bioinformatics *27*, 2987–2993. https://doi.org/10.1093/bioinformatics/btr509.
72. Love, M.I., Huber, W., and Anders, S. (2014). Moderated estimation of fold change and dispersion for RNA-seq data with DESeq2. Genome Biol. *15*, 550. https://doi.org/10.1186/s13059-014-0550-8.
73. Finn, R.D., Clements, J., and Eddy, S.R. (2011). HMMER web server: interactive sequence similarity searching. Nucleic Acids Res. *39*, W29–W37. https://doi.org/10.1093/nar/gkr367.
74. Botas, J., Rodríguez del Río, Á., Giner-Lamia, J., and Huerta-Cepas, J. (2022). GeCoViz: genomic context visualisation of prokaryotic genes from a functional and evolutionary perspective. Nucleic Acids Res. *50*, W352–W357. https://doi.org/10.1093/nar/gkac367.
75. Sörensen, M., Mak, T.N., Hurwitz, R., Ogilvie, L.A., Mollenkopf, H.J., Meyer, T.F., and Brüggemann, H. (2010). Mutagenesis of Propionibacterium acnes and analysis of two CAMP factor knock-out mutants. J. Microbiol. Methods *83*, 211–216. https://doi.org/10.1016/j.mimet.2010.09.008.
76. Casini, A., MacDonald, J.T., De Jonghe, J., Christodoulou, G., Freemont, P.S., Baldwin, G.S., and Ellis, T. (2014). One-pot DNA construction for synthetic biology: the Modular Overlap-Directed Assembly with Linkers (MODAL) strategy. Nucleic Acids Res. *42*, e7. https://doi.org/10.1093/nar/gkt915.

77. Pronobis, M.I., Deuitch, N., and Peifer, M. (2016). The Miraprep: A Protocol that Uses a Miniprep Kit and Provides Maxiprep Yields. PLoS One *11*, e0160509. https://doi.org/10.1371/journal.pone.0160509.

78. Rikken, G., Niehues, H., and van den Bogaard, E.H. (2020). Organotypic 3D Skin Models: Human Epidermal Equivalent Cultures from Primary Keratinocytes and Immortalized Keratinocyte Cell Lines. In Molecular Dermatology: Methods and Protocols, N.V. Botchkareva and G.E. Westgate, eds. (Springer), pp. 45–61. https://doi.org/10.1007/978-1-0716-0648-3_5.

79. Livak, K.J., and Schmittgen, T.D. (2001). Analysis of relative gene expression data using real-time quantitative PCR and the 2(-Delta Delta C(T)) Method. Methods *25*, 402–408. https://doi.org/10.1006/meth.2001.1262.

80. Roncarati, D., and Scarlato, V. (2017). Regulation of heat-shock genes in bacteria: from signal sensing to gene expression output. FEMS Microbiol. Rev. *41*, 549–574. https://doi.org/10.1093/femsre/fux015.

81. Patel, H., Ewels, P., Peltzer, A., Hammarén, R., Botvinnik, O., Sturm, G., Moreno, D., and Vemuri, P., silviamorins, Pantano, L., et al. (2020). nf-core/rnaseq: nf-core/rnaseq v3.0 – Silver Shark. Zenodo. https://doi.org/10.5281/ZENODO.4323183.

82. Zhai, W., Duan, Y., Zhang, X., Xu, G., Li, H., Shi, J., Xu, Z., and Zhang, X. (2022). Sequence and thermodynamic characteristics of terminators revealed by FlowSeq and the discrimination of terminators strength. Synth. Syst. Biotechnol. *7*, 1046–1055. https://doi.org/10.1016/j.synbio.2022.06.003.

## STAR★METHODS

### KEY RESOURCES TABLE

| REAGENT or RESOURCE | SOURCE | IDENTIFIER |
|---|---|---|
| **Antibodies** | | |
| Mouse anti-His antibody | Bio-Rad | Cat# MCA1396GA; RRID: AB_566361 |
| Horseradish peroxidase-coupled anti-mouse antibody | SantaCruz | Cat# sc516102; RRID: AB_2687626 |
| **Bacterial and virus strains** | | |
| *E. coli* NZYα | NZYTech | MB01008 |
| *E. coli* EC-24 | Knödlseder et al.[31] | CECT30749 |
| *C. acnes* KPA171202 | DSMZ | DSM 16379 |
| *C. acnes* 09-9 | Davidsson et al.[43] | RefSeq GCF_002600615.1 |
| *C. acnes* AD24 | Lood et al.[64] | N/A |
| *C. acnes* H1 Lab isolate | Lab collection | N/A |
| *C. acnes* KPA171202 ΔLysA | This study | N/A |
| *C. acnes* KPA171202 ΔHisB | This study | N/A |
| *C. acnes* KPA171202 ΔProA | This study | N/A |
| **Chemicals, peptides, and recombinant proteins** | | |
| Brucella Medium | Condalab | 1012 |
| GasPak EZ Anaerobe Pouch System | BD | BD260683 |
| AnaeroGen System | Thermo Scientific | AN0025A |
| Brain-heart infusion (BHI) Medium | Condalab | 1400 |
| DMEM F-12 medium lacking aminoacids and glucose (see Table S1 for the full components list used for this media) | US Biological | D9807-02A |
| KAPA HiFi | Roche | KK2601 |
| Phanta Max | Vazyme | 001 |
| NuPAGE 4-12% gel | Invitrogen | NP0322BOX |
| Immobilon-P Transfer Membrane | Merck Millipore | IPVH00010 |
| Tris buffered saline | Bio-Rad | 1706435 |
| Pierce ECL Western Blotting Substrate | Thermo Fisher Scientific | 32106 |
| EpiLife medium | Gibco | MEPI500CA |
| Human keratinocyte culture supplement (HKGS) | Gibco | S0015 |
| CnT-Prime | CELLnTEC | CNT-PR |
| Hanks' balanced salt solution (HBSS) | Capricorn Scientific | HBSS-2A |
| 6-chloromethyl-2',7'-dichlorodihydrofluorescein diacetate (CM-H2DCFDA) | Invitrogen | C6827 |
| DNaseI | Invitrogen | 18068015 |
| PowerUp SYBR Green Master Mix | Life Technologies | A25742 |
| 2,4-Diacetylphloroglucinol (DAPG) | Cayman Chemical | 16345 |
| Anhydrotetracycline hydrochloride (aTc) | Sigma | 94664-10MG |
| **Critical commercial assays** | | |
| QIAquick PCR purification | Qiagen | 28104 |
| QIAquick gel extraction | Qiagen | 28704 |
| NZYMiniprep kit | NZYTech | MB01008 |
| PureLink Maxiprep kit | Invitrogen | K210017 |
| SOD activity assay kit | Sigma | CS0009 |
| E.Z.N.A. Total RNA kit | Omega bio-tek | R6834-02 |
| RevertAid First Strand cDNA Synthesis kit | ThermoFisher | K1622 |

(*Continued on next page*)

*Continued*

| REAGENT or RESOURCE | SOURCE | IDENTIFIER |
|---|---|---|
| Deposited data | | |
| RNA-seq Data | This study | ENA: PRJEB78978 |
| See Data S1 for all plasmid sequences (GeneBank format) used in this study | This study | N/A |
| Experimental models: Cell lines | | |
| N/TERT-2G | Dickson et al.[62] | N/A |
| Oligonucleotides | | |
| See Table S2 for a full list of oligonucleotides used in this study | This study | N/A |
| Recombinant DNA | | |
| See Table S3 for a full list of plasmids used in this study | This study | N/A |
| Software and algorithms | | |
| FlowJo | Treestar | https://www.flowjo.com/ |
| R | R Core Team | https://www.r-project.org/ |
| flowCore package | Hahne et al.[65] | https://doi.org/10.18129/B9.bioc.flowCore |
| changepoint package | Killick and Eckley[66] | https://github.com/rkillick/changepoint |
| nf-core RNA-seq pipeline v3.0 | Ewels et al.[67] | https://github.com/nf-core/rnaseq |
| Nextflow v20.12.0-edge | Di Tommaso et al.[68] | https://www.nextflow.io/ |
| Trim Galore v0.6.6 | Babraham Institute | https://www.bioinformatics.babraham.ac.uk/projects/trim_galore/ |
| STAR v2.6.1d | Dobin et al.[69] | https://github.com/alexdobin/STAR |
| SAMtools v1.10 | Li et al.[70] | https://www.htslib.org/ |
| FastQC v0.11.9 | Babraham Institute | https://www.bioinformatics.babraham.ac.uk/projects/fastqc/ |
| BCFtools in v1.16 | Li[71] | https://samtools.github.io/bcftools/ |
| DeSeq2 | Love et al.[72] | https://bioconductor.org/packages/release/bioc/html/DESeq2.html |
| R Scripts for Data Analysis and plotting | This study | https://doi.org/10.5281/zenodo.14346074 |
| HMMscan | Finn et al.[73] | https://www.ebi.ac.uk/Tools/hmmer/search/hmmscan |
| GeCoViz | Botas et al.[74] | https://gecoviz.cgmlab.org/ |
| Other | | |
| Amicon ultra 0.5mL 30K centrifugal filters | Millipore | UFC503096 |
| 1 mm electroporation cuvette | Bio-Rad | 1652089 |
| Precellys 0.1 mm silica beads | VWR | 432-3754 |

## EXPERIMENTAL MODEL AND STUDY PARTICIPANT DETAILS

### Microbial strains and media

*C. acnes* KPA171202 was obtained from the German Collection of Microorganisms and Cell Cultures (DSMZ: DSM16379). *C. acnes* strain 09-9[43] (GenBank: GCA_002600615.1) was kindly provided by Dr. Holger Brüggemann. *C. acnes* strain AD24[64] was kindly provided by Dr. Rolf Lood. All *C. acnes* strains were grown in Brucella agar plates (1012, Condalab) at 37 °C in anaerobic conditions generated either with the GasPak EZ anaerobe pouch system (BD260683, BD) or the AnaeroGen System (AN0025A, Thermo Scientific). For liquid cultures, a starting culture of 0.1 $OD_{600}$ was inoculated in brain-heart infusion (BHI) media (1400, Condalab) and grown at 37 °C 110 r.p.m. in anaerobic conditions. Unless otherwise indicated, cultures were generally grown for 24h (i.e. exponential phase) to perform the experiment. When appropriate, plates or liquid cultures were supplemented with either 5 μg $mL^{-1}$ chloramphenicol or 10 or 50 μg $mL^{-1}$ erythromycin. For measuring promoter and RBS strength in stationary phase, cultures were grown for 4 days. For the synthetic sensors, liquid cultures were incubated in the presence (or absence) of 100 ng $mL^{-1}$ aTC or 5 μM DAPG for 3.5 or 5 days, respectively.

For the experiments involving auxotrophies, *C. acnes* was grown using defined synthetic media based on DMEM F-12 medium lacking amino acids and glucose (D9807-02A, US Biological) supplemented with 3.151 g $L^{-1}$ glucose and 1.2 g $L^{-1}$ sodium bicarbonate. The pH was adjusted to 6 with HCl and the media sterilized with a 0.2 μm filter. All amino acids were autoclaved and added unless indicated.

*C. acnes* cultures were inoculated as previously mentioned with a starting $OD_{600}$ of 0.1. and grown in anaerobic conditions. All media components per L are indicated in Table S1. To evaluate the auxotrophies, all aminoacids were added to the basal media except for the one being tested. For instance, to evaluate histidine auxotrophy, the basal medium was supplemented with all amino acids except histidine and growth was measured both in the absence and presence of histidine. For the calculation of relative reduction in $OD_{600}$, the $OD_{600}$ reported in the condition without amino acid was subtracted to the $OD_{600}$ in the condition with amino acid and the result was divided by the $OD_{600}$ in the condition with amino acid (% Reduction = ($OD_{600}$ aa' - $OD_{600}$ w/o aa')/$OD_{600}$ aa').

For plasmid curation, cells were passaged twice by replating them in Brucella agar plates without the selecting antibiotic. Cells were then resuspended in BHI and serial dilutions were performed in order to obtain single colonies after plating. Plates with individual colonies were replica-plated in a Brucella agar plate with the appropriate antibiotic to identify colonies that had lost the plasmid.

## METHOD DETAILS

### Plasmids and molecular biology

All plasmids in this study were based on the *Propionibacterium freudenreichii* replicative vector pBRESP36A[35,36] or on a pUC-19 based suicide vector for homologous recombination[75] (Table S3). PCR fragments were usually amplified with either KAPA HiFi (KK2601, Roche) or Phanta Max (001, Vazyme) and purified using QIAquick PCR purification or gel extraction kits (28104/28704, Qiagen). Plasmids were built using a modular Gibson-based cloning method.[37] The method consists of two steps: step 1 relies on Gibson assembly of transcriptional units into individual intermediate plasmids; in step 2, these plasmids are digested, which generates flanking regions containing overlaps that drive a second Gibson assembly, thus yielding the final construct. For step 1, all DNA parts were flanked by the same Prefix (CAGCCTGCGGTCCGG) and Suffix (TCGCTGGGACGCCCG) sequences.[76] Basically, For and Rev primers annealing to Prefix and Suffix sequences, respectively, were used for PCRs that added unique linkers to the DNA parts (Table S2, Cloning primers). PCR amplifications were column-purified as specified above and assembled using a custom Gibson enzyme mix (Centre de Regulación Genomica CRG, 1 h 50 °C) into backbones previously digested with the appropriate restriction enzymes (NEB, 1 h 37 °C) to generate the intermediate plasmids. In step 2, these intermediate plasmids were digested with enzyme combinations that produced overlapping ends, purified, and assembled as described above to yield the final constructs. Plasmids were transformed into chemically competent *E. coli* DH5$\alpha$ (MB00402, NZYtech) and plated in LB agar plates with the appropriate antibiotic (50 $\mu$g $mL^{-1}$ Ampicillin, 50 $\mu$g $mL^{-1}$ Kanamycin, 50 $\mu$g $mL^{-1}$ Spectinomycin or 25 $\mu$g $mL^{-1}$ Chloramphenicol). Liquid cultures were made in LB and incubated at 37°C 220 r.p.m. for plasmid extraction using the NZYMiniprep kit (MB01008, NZYtech). Purified plasmids were sequenced using backbone-annealing primers by Sanger sequencing (Genewiz) (Table S2, Sequencing primers). Following sequence verification, plasmids were shuttled through *E. coli* EC-24[31] (#CE9CT30749 of the Spanish Type Culture Collection), which is a *Δdam Δdcm ΔhsdMS* strain harbouring the *C. acnes* IIIB methylase; this strain provides plasmids with the *C. acnes* DNA methylation pattern and therefore prevents plasmid degradation by the *C. acnes* endogenous R-M system upon transformation. Plasmids shuttled through EC-24 were then extracted either through the NZYMiniprep kit, the Miraprep protocol[77] or the PureLink Maxiprep kit (K210017, Invitrogen) to obtain enough DNA mass for electroporation. When necessary, plasmids were washed with the Amicon ultra 0.5 mL 30K centrifugal filters (UFC503096, Millipore) according to manufacturer's instructions to avoid arcing during the electroporation. Sequence-verified, purified plasmids containing the *C. acnes* methylation pattern were ready for transformation into *C. acnes* cells.

### *C. acnes* electrocompetent cell preparation and transformation

*C. acnes* electrocompetent cells were prepared as previously described.[31] Briefly, *C. acnes* starting inocula of 0.1 $OD_{600}$ were grown for 24h until ~1 $OD_{600}$. Then, cells were treated with 0.4 M Sucrose and 10 $\mu$g $mL^{-1}$ penicillin G for 5h. Afterwards, cells were centrifuged at 2367 r.c.f. for 10 minutes at 4°C and resuspended in electroporation buffer consisting of 272 mM sucrose, following a second centrifugation with the same conditions. Cells were resuspended in 1 mL and transferred to a 1.5 mL microcentrifuge tube where they were washed at 1657 r.c.f. for 10 minutes followed by 4 washes at 9391 r.c.f. for 1 minute each. After the last wash, cells were resuspended in electroporation buffer supplemented with 10% glycerol, washed once again at 9391 r.c.f. for 1 minute and resuspended in 50 $\mu$L of electroporation buffer with 10% glycerol per 50 mL of starting culture volume. Finally, cells were frozen in liquid nitrogen and stored at -75°C for later use. For transformation, a cell aliquot was slowly thawed on ice, resuspended in 1 mL electroporation buffer and centrifuged at 9391 r.c.f. for 1 minute. After resuspension in the same initial volume with electroporation buffer, cells were diluted four times with electroporation buffer to a final volume of 40 $\mu$L and either 1000 ng of DNA were added for replicative plasmid transformation or 8000 ng for the suicide vectors. For electroporation, the mixture was transferred to a precooled 1 mm electroporation cuvette (1652089, Bio-Rad) and electroporated at 1.5 kV, 25 $\mu$F and 400 $\Omega$. Immediately after the pulse, cells were resuspended in 100 $\mu$L of BHI medium and plated on Brucella agar plates for 24 h recovery at 37 °C in anaerobic conditions. Next day, cells were collected with a cotton swab, resuspended in 1 mL BHI, centrifuged at 1657 r.c.f. for 5 minutes, resuspended in 100 $\mu$L BHI and plated on 2 Brucella agar plates supplemented with the appropriate antibiotic for a 6-day incubation in anaerobic conditions at 37 °C.

### Immunodetection of secreted SOD

Liquid cultures of recombinant *C. acnes* were grown in selective media for two days, in the case of constitutive expression, or four days, for inducible expression. For inducible expression, the cultures were initially split in two and one of the halves was induced with 100 ng $mL^{-1}$ anhydrotetracycline (aTc). Bacteria were collected by centrifugation at 10000 r.c.f. for 15 min and the pellet (cell

fraction, C) was lysed using Precellys 0.1 mm silica beads (432-3754, VWR) and resuspended in Bolt LDS Sample buffer (Thermo Fisher Scientific) containing 5% beta-mercaptoethanol. The supernatant (SN) containing the secreted SOD was subjected to trichloroacetic acid (TCA) precipitation: samples were precipitated in 10% trichloroacetic acid for 30 min on ice, and precipitates were pelleted by centrifugation at ~10,000 r.c.f. for 15 min at 4 °C. The pellets were washed twice with 500ul cold (−20 °C) acetone, air-dried, and resuspended in Bolt LDS Sample buffer with 5% beta-mercaptoethanol. Cell and supernatant samples were boiled at 98 °C for 10 min, and equal amounts of C and SN fractions were analysed using SDS-PAGE and His-tag immunodetection. Briefly, a NuPAGE 4-12% gel (NP0322BOX, Invitrogen) was run at 120 V for 1 h 30 min - 1 h 45 min, and proteins were transferred onto a PVDF membrane (IPVH00010, Immobilon-P Transfer Membrane, Merck Millipore) using a wet blotting apparatus running at 20 V for 1 h. Membranes were blocked (1 h at room temperature or overnight at 4 °C) with 4% milk in TBST (Tris buffered saline (1706435, Bio-Rad) containing 0.05% Tween 80) and incubated (1 h at room temperature or overnight at 4 °C) with mouse anti-His antibody (MCA1396GA, Bio-Rad) diluted 1:800 in TBST-4% milk. Following three 10 min washes in TBST, membranes were incubated for 1 h in horseradish peroxidase-coupled anti-mouse antibody (sc516102, SantaCruz) diluted 1:1000 in TBST-4% milk, and washed again three times 10 min each in TBST. Membranes were developed with Pierce ECL Western Blotting Substrate (32106, Thermo Fisher Scientific) and recorded using a ChemiDoc MP Imaging System (Bio-Rad).

### N/TERT-2G cell culture, UV-exposure and AD monolayer model

The immortalized keratinocyte cell line N/TERT-2G[61,62] was obtained from the J. Rheinwald laboratory (Harvard Medical School, Boston, USA). These cells were passaged in T25 or T75 flasks in keratinocyte-serum free EpiLife medium (MEPI500CA, Gibco) with human keratinocyte culture supplement (HKGS) (S0015, Gibco) based on previously published protocols[78] in a humidified 5% $CO_2$ incubator. Alternatively, CnT-Prime (CNT-PR, CELLnTEC) media was also used.

For UV-exposure, cells were seeded at 3.6 x $10^4$ cells $mL^{-1}$ in 24 well plates. When confluent, cells were exposed for 30 minutes to four UV-B lamps (302 nm) (Gel Dock XR+, Biorad). Then, cells were washed with Hanks' balanced salt solution (HBSS) (HBSS-2A, Capricorn Scientific) and dyed for 30 minutes at 37 °C with 20 μM 6-chloromethyl-2',7'-dichlorodihydrofluorescein diacetate (CM-H2DCFDA) (C6827, Invitrogen). After washing again with HBSS, we applied the 0.2 μm filtered bacterial supernatant for 5h on the cells, and we measured the ROS levels using a M Nano Infitine 200 Pro plate reader (Tecan) at an excitation/emission of 485/535nm.

### RNA extraction

Total RNA was isolated by E.Z.N.A. Total RNA kit (R6834-02, Omega bio-tek). For bacterial RNA isolation, cultures were centrifuged at 8000 r.c.f. for 5 minutes and resuspended in 1 mL TRK Lysis buffer. Then, cells were lysed using Precellys 0.1 mm silica beads (432-3754, VWR) for 15 minutes in a Disruptor Genie (SI-D258, Scientific Industries) and the supernatant was collected after centrifugation for 4 minutes at 10.000 r.c.f. for further processing. For human RNA isolation, 350 μL of TRK lysis buffer was added directly to cells and taken for further processing according to manufacturer's instructions. Briefly, extracted RNA in TRK buffer was mixed with an equal volume of fresh ethanol 70% and loaded in the RNA isolation columns by centrifugation at 13.000 r.c.f. for 1 minute. Then columns were washed with 500 μL of Wash Buffer I, 500 μL of Wash Buffer II twice and a last 2 minute centrifugation to let the column dry. The RNA was eluted with 40 μL RNase free water and concentration was measured with NanoDrop One Spectrophotometer (ND-ONE-W, ThermoFisher)

### RT-qPCR

500 ng of isolated total RNA were treated with DNaseI (18068015, Invitrogen) and used for cDNA synthesis using the RevertAid First Strand cDNA Synthesis kit (K1622, ThermoFisher) according to the manufacturer's protocols. Subsequent real-time quantitative PCR (RT-qPCR) was performed using PowerUp SYBR Green Master Mix (A25742, Life Technologies). Target gene expression levels were normalized using the housekeeping gene gyrase B (GyrB) from *C. acnes*. The ΔΔCT method was used to calculate relative mRNA expression levels.[79] All primers used are described in Table S2.

### Homology search

We identified candidates for temperature sensing transcription factors among the differentially expressed genes obtained from the RNA-seq. We manually used HMMscan[73] to identify conserved domains in potential candidates and compared them with the domains of known transcription factors related to temperature sensing in the literature.[80] Then, we examined operon conservation using GeCoViz[74] and manually evaluated the domains shared between *C. acnes* potential homologs and reported heat-shock operon genes described in the literature[80] using HMMScan.

## QUANTIFICATION AND STATISTICAL ANALYSIS

### Flow cytometry

*C. acnes* cells were analysed by flow cytometry on a LSR Fortessa 4L analyzer (BD) with a 488 nm laser and 530/30 band pass filter for sfGFP, mCitrine and pFAST-Lime, a 405 nm laser with a 450/50 nm band pass filter for Cerulean, and a 561 nm laser with either a 610/20 band pass filter for EforCP and mCherry or a 585/15 nm for mKO2. For the terminator assay, cells were analysed on Attune Nxt flow cytometer (Invitrogen) using a 488 nm laser and a 530/30 nm band-pass filter for sfGFP, and a 561 nm laser together with a 620/15 nm filter for mCherry. Cells were centrifuged at 1657 r.c.f for 5 minutes and resuspended in PBS to ensure separation of

cell events. FSC-H and SSC-H thresholds were set to exclude background events. Data was analysed using either FlowJo software (Treestar) or a custom R script using the *flowCore* package.[65] The fluorescence median of each gated population was calculated and reported in this publication as the fluorescence value of a sample in arbitrary units (a.u.). This median was always calculated as the median of the whole population unless otherwise indicated. For the experiment measuring the different reporters (Figure 1D) and the experiment measuring mCherry with different *C. acnes* strains (Figure 1H), we defined an arbitrary threshold to select the populations clearly more fluorescent than the negative control and reported the median fluorescence intensity of these selected populations for each strain (Figures S2 and S7).

### RNA-seq

Isolated RNA was analyzed for purity and integrity using Bioanalyzer (Agilent Technologies GmbH, Germany). Library construction and RNA-sequencing was performed by Macrogen Inc. (Seoul, South Korea) using the Truseq Stranded Total RNA and sequenced using an Illumina at 60M pair-reads depth. RNA-seq analysis was performed using the nf-core RNA-seq pipeline v3.0[67,81] in Nextflow v20.12.0-edge.[68] Raw paired-end reads were trimmed using Trim Galore v0.6.6 and aligned to the C. acnes KPA171202 reference genome (Genbank AE017283) using STAR v2.6.1d[69] and SAMtools v1.10.[70] Quality control was performed using FastQC v0.11.9. Mapped reads were counted using mpileup from BCFtools in htslib v1.1.[71] For temperature-sensitive promoters, differential gene expression analysis between two heat shock samples and two controls was performed on the normalized read counts using DeSeq2.[72] Genes with a log fold-change greater than 3 were selected for further manual inspection of the read coverage across the genetic locus. We extracted either 200 bp upstream the start codon or the whole intergenic region for those genes whose upregulation was consistent all over their ORF. Similarly, constitutive promoters were selected among the genes within the 15% lowest variation coefficient (CV) and after manual inspection of the read coverage for uniformity. Again, the regulatory sequence was identified as either the intergenic region or 200 bp upstream from the start codon. For endogenous terminator sequences, mean change points were detected across the coverage pileup using the changepoint R package *cpt.mean*.[66] Then, we calculated the segments between change points and selected those segments containing at least one stop codon that had the greatest drop in expression compared with their neighbouring segments. After manual inspection of those segments fulfilling these criteria, we selected as terminator sequences the intergenic regions within the selected segments.

### SOD activity quantification

0.2 μm-filtered *C. acnes* supernatants were transferred to a 96-well plate to measure the SOD activity using an SOD activity assay kit (CS0009, Sigma) following manufacturer's instructions. Briefly, 20 μL from supernatants were mixed with 160 μL of the WST dye, and 20 μL of xanthine oxidase were added to start the reaction. The SOD activity was calculated using a standard calibration curve. First, the absorbance at 450 nm from each sample was averaged across replicates. To obtain the linearized SOD rate, a blank control was subtracted from all samples and standards, and resulting values were divided by the absorbance of the control reaction lacking SOD. The standards were then used for a linear regression to obtain the calibration parameters as the slope and intercept. Then the following formula was applied.

$$SOD\ activity\ (units\ /\ mL) = \frac{SampleLSR - intercept}{Slope} \times 10$$

Where $Sample_{LSR}$ is the linearized SOD rate of the sample and the multiplication by 10 corresponds to the dilution factor. A calibration curve was only considered valid when its $R^2$ was higher than 0.95.

### Statistics and reproducibility

Statistical analysis was performed using R and RStudio. Each experiment includes at least three independent replicates and graphs include the mean ± s.d. Unpaired one-way analysis of variance (ANOVA) was used for comparison between multiple groups followed by Tukey's multiple comparison post hoc unless specified in the figure legend. Results with p-value < 0.001 were considered highly statistically significant (***). Results with p-value < 0.05 were considered as significant (*). All blots and gels were repeated at least two times.

Terminator efficiency (Figure S7) was calculated with the following equation as previously described.[82]

$$Terminator\ efficiency = 1 - \left(\frac{mCherry\ Terminator}{mCherry\ Spacer_1}\right) \Big/ \left(\frac{sfGFP\ Terminator}{sfGFP\ Spacer_1}\right)$$

Where Spacer_1 corresponds to the mCherry or the sfGFP fluorescence levels from the control harbouring only the Spacer_1 sequence and no terminator, and Terminator corresponds to the fluorescence levels of the terminator evaluated. Error bars were calculated with the following formula, propagating the error of three biological replicates:

$$Propagated\ error = \sqrt{\left(\frac{\sigma_{mCherry\ Ratio}}{GFP\ Ratio}\right)^2 + \left(\frac{mCherry\ Ratio \times \sigma_{GFPRatio}}{GFP\ Ratio^2}\right)^2}$$